Evidence for noncollective oblate structures at high spin in ^{123}Cs

A. K. Singh,* H. Hübel, and J. Domscheit
Helmholtz-Institut für Strahlen-und Kernphysik, Universität Bonn, Nussallee 14-16, D-53115 Bonn, Germany

G. B. Hagemann, B. Herskind, D. R. Jensen, and J. N. Wilson†
Niels Bohr Institute, Blegdamsvej 17, KD-2100 Copenhagen Ø, Denmark

R. Clark, M. Cromaz, P. Fallon, A. Görgen,‡ I. Y. Lee, A. O. Macchiavelli, and D. Ward
Nuclear Science Division, Lawrence Berkeley National Laboratory, Berkeley, California 94720, USA

H. Amro§ and W. C. Ma
Department of Physics, Mississippi State University, Mississippi State, Mississippi 39762, USA

J. Timár
Institute of Nuclear Research of the Hungarian Academy of Sciences, H-4001 Debrecen, Hungary

I. Ragnarsson
Department of Mathematical Physics, Lund Institute of Technology, Box 118, S-221-Lund, Sweden
(Received 26 May 2004; published 28 September 2004)

High-spin states in ^{123}Cs were populated in the ^{64}Ni(^{64}Ni,$p4n$) reaction at a beam energy of 265 MeV. Gamma-ray coincidences were measured using the Gammasphere spectrometer. Two additional bands have been placed in the level scheme and the four previously known bands have been extended to higher spin. At the highest spins, two of the bands show irregular level sequences. These structures of noncollective excitations, which compete with collective rotation, are interpreted as band-terminating states. The results are compared to cranked Nilsson-Strutinsky calculations, and configuration assignments to the bands and to the terminating states are discussed.

DOI: 10.1103/PhysRevC.70.034315 PACS number(s): 23.20.Lv, 23.20.En, 27.60.+j, 21.60.Ev

I. INTRODUCTION

Neutron-deficient nuclei in the mass 125 region are soft to γ-deformation at low and medium spin. They provide a platform to study the development of collectivity and nuclear shape with increasing spin and as a function of nucleon number. The shape-driving properties of the neutrons and protons in the unique-parity $h_{11/2}$ intruder orbital are well known in this region [1,2]. The proton Fermi surface lies low within the $h_{11/2}$ multiplet, which drives the nucleus towards prolate shape, whereas the neutron Fermi surface lies near the middle of the $h_{11/2}$ subshell, which tries to drive the shape towards oblate. Shape changes are expected to occur, in particular due to the alignment of pairs of either protons or neutrons in the $h_{11/2}$ orbitals.

Total routhian surface calculations employing a deformed Woods-Saxon potential and a monopole pairing residual interaction have been performed to explore systematic trends in this mass region [1,2]. These calculations show that the alignment of protons and neutrons drives the nuclei towards triaxiality with different values of γ. Small positive values around $\gamma \simeq 0$ are favored after the proton alignment, whereas negative γ values, around $\gamma = -30°$, are preferred due to the neutron alignment. A transition from prolate shape at low spin to oblate deformation at high spin via an intermediate triaxial shape has been systematically predicted by these calculations [3].

High-spin studies in neutron-deficient I (e.g., Refs. [4–7]) and Xe [3,8,9] nuclei have revealed the presence of irregular structures on top of regular rotational bands. These observations were interpreted as band termination. In a terminating band [10], the structure changes and the deformation develops from prolate shape, rotating about an axis perpendicular to the symmetry axis, through a sequence of triaxial shapes to an oblate shape, symmetric around the rotation axis, where single-particle excitation is the cheapest way to generate angular momentum. The bands terminate at the maximum spin which can be obtained by aligning the angular momenta of all the particles involved in a particular configuration. Higher-spin states above the terminating state, can be obtained by breaking the core and aligning the single-particle angular momenta along the rotation axis.

In the Cs isotopes with $Z=55$, which lie in this mass region, band termination is also expected to occur at high spin. In this context, it is interesting to explore the analogous

*Present address: Department of Physics, IIT Kharagpur, Kharagpur-721302, India.
†Present address: LPSC/IN2P3, F-38026, Grenoble Cedex, France.
‡Present address: DAPNIA/SPhN, CEA-Saclay, F-91191 Gif-sur-Yvette, France.
§Present address: WNSL, Yale University, New Haven, CT 06520-8124.

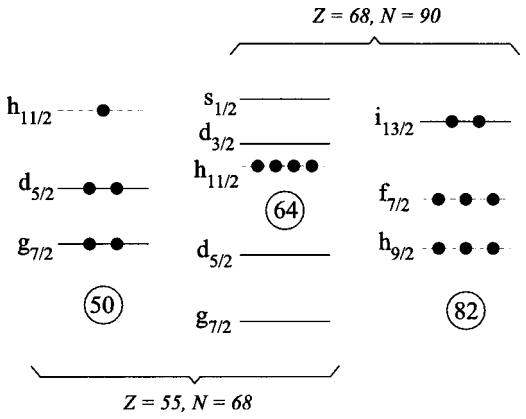

FIG. 1. The analogous filling of subshells in configurations with a few particles outside ^{114}Sn and ^{146}Gd is illustrated. Combining the $Z=55$ structure (left) with the $N=68$ structure (middle) results in a configuration for ^{123}Cs with $I_{\max}=63/2^-$, while a combination of the $Z=68$ proton structure (middle) with the $N=90$ neutron structure (right) corresponds to the band terminating at $I=46$ in ^{158}Er. Note that the $Z=55$ and the $N=90$ configurations have both approximately ten times more core particles than valence particles.

features between the Xe/Cs/Ba nuclei with $N=66-68$ and the Dy/Er nuclei with $N=88-90$, as previously pointed out in Ref. [11]. As illustrated in Fig. 1, these nuclei have a few valence neutrons and valence protons, respectively, in the $h_{11/2}$ subshell above the "semi-magic" gap at particle number 64. This structure is combined with configurations with a limited number of protons or neutrons outside the magic $Z=50$ and $N=82$ gaps, respectively. In the specific example chosen in Fig. 1, the $(h_{11/2})^4$ configuration with a maximum spin of $16\,\hbar$ is combined with either a proton $(g_{7/2}d_{5/2})^4(h_{11/2})^1$ or a neutron $(h_{9/2}f_{7/2})^6(i_{13/2})^2$ configuration with $I_{max}=15.5$ and $30\,\hbar$, respectively. Thus, a predicted terminating state at $I^\pi=63/2^-$ in ^{123}Cs becomes analogous to the $I^\pi=46^+$ state in ^{158}Er [11,12]. While the latter corresponds to the first terminating state observed in the $A=158$ region, the former is now observed according to our assignments below.

Prior to this work, high-spin states in ^{123}Cs were studied through in-beam experiments using small detector arrays [13–15]. However, no evidence for band-terminating structures was observed in these studies. The aim of the present work was to look for such noncollective structures possibly becoming yrast at very high spin.

In this article we report on results of an in-beam study on ^{123}Cs using the Gammasphere spectrometer. Six bands have been placed in the level scheme. All the known bands have been extended to higher spin. In two of the bands, irregular structures have been observed, most probably due to noncollective excitations.

II. EXPERIMENTAL PROCEDURE

High-spin states ^{123}Cs were populated in the ^{64}Ni(^{64}Ni, $p4n$) reaction at a beam energy of 265 MeV. The beam was provided by the 88 in. cyclotron at Lawrence Berkeley National Laboratory. The γ rays following the reaction were detected by the Gammasphere spectrometer array. At the time of experiment the array was equipped with 100 Compton-suppressed Ge detectors. The ^{64}Ni target was a foil of 0.476 mg/cm^2 thickness enriched to 96.5%. The data were written to tape in list mode with the condition that six or more Compton-suppressed Ge detectors, and 15 or more "modules" were in coincidence. A module is defined as a unit consisting of a Ge detector together with the Bismuth Germinate (BGO) scintillators surrounding the Ge crystal which act as an anti-Compton shield. After presorting and setting prompt time gates a total of 1.2×10^9 events with Ge-fold $\geqslant 4$ remained for further analysis.

The primary goal of this experiment was to search for hyperdeformation. The beam energy and the trigger condition on high Ge-fold were chosen to enhance the population and selection of hyperdeformed structures in ^{126}Ba. A number of reaction channels were open at this beam energy, the dominant channels were $4n$, $\alpha 2n$, $3n$, $p3n$, $p2n$, and $p4n$ with relative intensities of 100, 95, 51, 36, 24, and 20, respectively.

The calibrated γ-ray energies were corrected for Doppler shifts according to the angular position of the detectors, Due to the high velocity of the recoiling nuclei ($v/c\simeq 4.4\%$), it is necessary to include also the higher order terms in the Doppler-correction formula. The coincidence events were unpacked and sorted into three- and four-dimensional arrays, cubes, and hypercubes, respectively, using the program package RADWARE [16].

DCO ratios, defined as

$$R_{\mathrm{DCO}}=\frac{I(\gamma_2^{35^\circ},\gamma_1^{90^\circ})}{I(\gamma_2^{90^\circ},\gamma_1^{35^\circ})},$$

where $I(\gamma_2,\gamma_1)$ denotes the intensity of γ_2 with a gate set on γ_1, were determined from E_γ–E_γ matrices with events detected in forward and backward detectors, close to average angles of 35° and 145°, on one axis and those detected in detectors close to 90° on the other axis. The DCO ratios for γ-ray transitions were obtained by setting gates on stretched $E2$ transitions. Typical values of the DCO ratio are 1.0 and 0.5 for stretched quadrupole and dipole transitions, respectively.

Alternatively, angular distribution matrices were sorted with the condition that in one matrix events detected in detectors close to 35° or 145° were placed on one axis and those in all detectors on the other axis. Similarly the second matrix was created with events detected in detectors which are close to 90° on one axis and those in all detectors on other axis. Gates were set in these matrices on the axis with events detected in all detectors. The intensities of the transitions in the gated spectra can be used to distinguish between stretched dipole and quadrupole transitions. The advantage with the second method is that one can use the whole statistics, which is helpful in determining the multipolarity of weak transitions. Typical values of the intensity ratios for stretched quadrupole and dipole transitions for the current detector setup are around 1.45 and 0.7, respectively.

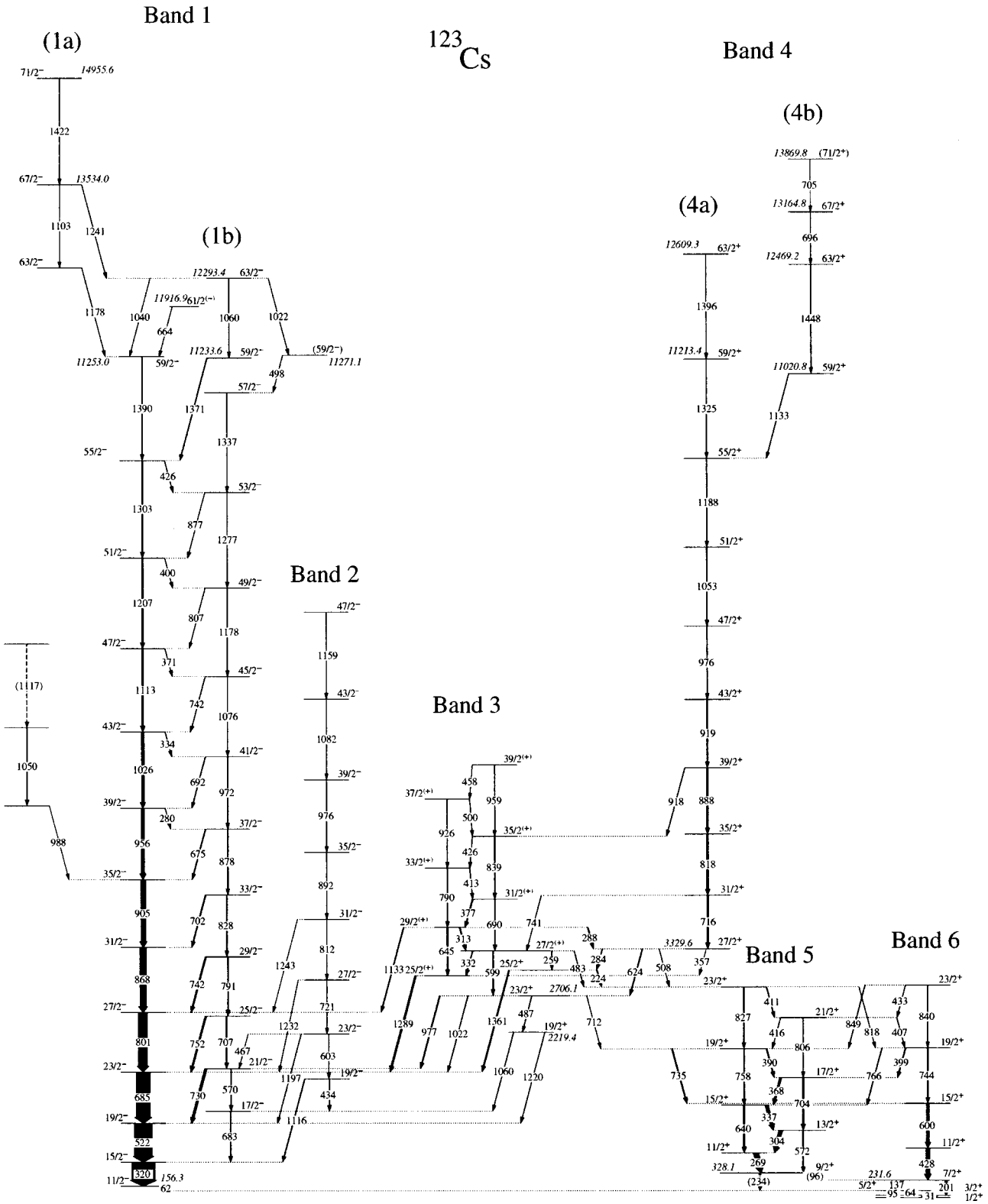

FIG. 2. The level scheme of ^{123}Cs.

III. EXPERIMENTAL RESULTS AND LEVEL SCHEME

The level scheme of ^{123}Cs, as shown in Fig. 2, has been constructed using coincidence relationships between γ-ray transitions and their intensities. Spins of the levels have been assigned on the basis of the DCO ratios. In some cases, the presence of crossover and interband transitions also helps in assigning the spins. The parity of the known bands has been adopted from previous work [14], whereas for the additional bands (3 and 4), assignments have been made on the basis of

the measured DCO ratios of the decay-out transitions connecting the additional bands to levels of known parity. For these assignments, it was assumed that stretched quadrupole transitions have $E2$ multipolarity (and not $M2$ which is very unlikely). The intensities, DCO ratios, and assignments of transitions in ^{123}Cs are listed in Table I.

The low-energy part of the level scheme had been established through radioactive decay studies [17–20]. Later, high-spin states including collective bands were established above these states through in-beam measurements [13–15]. Recently, low-lying structures in ^{123}Cs were investigated by Gizon *et al.* [21] by a radioactive decay study. Contradictory results were presented by these authors in assigning the excitation energies of some of the low-lying levels. Among the important modifications in the context of the present work are the excitation energies of the first $7/2^+$ and $9/2^+$ states. A collective band has been observed [14] on each of these states.

In this work, we have adopted the low-lying level structure from the work of Gizon *et al.* [21]. Six bands have been placed in the level scheme, in which two are new in the present work. The previously known bands 1, 2, and 6 have been extended to higher spins.

The excitation energy of the isomeric $11/2^-$ state, the band-head of band 1, was reported to be at 156.3 keV [20], which is confirmed by Gizon *et al.* [21]. The highest spin state of this band (with upper two as tentative transitions) assigned by Lidén *et al.* [15] was the $59/2^-$ level. In the present work, we confirm those tentative γ rays with energies of 1303.1 and 1371.0 keV and two additional structures consisting of two to three γ transitions have been established on top of them. Figure 3 shows a triple-gated spectrum for this band. The unfavored signature partner of this band which starts from the $17/2^-$ level was known up to the $33/2^-$ state [14]. We have extended this sequence by six transitions up to spin $57/2^-$. Furthermore, a number of additional γ rays connecting the unfavored and favored branches have been established. Five γ rays of energies 280.3, 334.2, 371.3, 400.0, and 426.5 keV have been observed to decay from the favored to the unfavored band at higher spin. Above spin $55/2$, the favored sequence forks into two parallel structures with two $59/2$ and two $63/2$ states, shown in Fig. 2 as structures 1a and 1b, respectively. Their placement is based on coincidence relationships and intensity balances. The placement is further supported by the observation of the 1040.5 and the 1240.5 keV γ rays connecting these two structures. The DCO ratios measured for the 1371.0 and 1390.3 keV γ rays show that they are stretched quadrupole transitions. Hence, spin $59/2$ has been assigned to the lowest states of structures 1a and 1b. DCO ratios could be measured for the γ rays of energies 1059.8, 1240.5, and 1421.7 keV, which show that they are stretched quadrupoles. Thus, spin $71/2$ could be assigned to the highest state of band 1. In all these assignments, negative parity has been assumed for the levels due to their decay to the negative-parity band 1.

A γ ray with an energy of 663.9 keV has been observed in coincidence with the 1390.3 keV transition, but not in coincidence with the γ ray of 1371.0 keV. The DCO ratio of 0.77(10) of the 663.9 keV transition clearly shows its dipole character and, hence, spin $61/2$ has been assigned to the level at 11916.9 keV. A decay path between the $63/2^-$ level of structure 1b and the $57/2^-$ state of the unfavored sequence has been established through the transitions of 498.0 and 1022.3 keV. The ordering of these transitions is tentative. The DCO ratio measured for the 498.0 keV γ ray shows that it is a mixed $M1/E2$ transition and, therefore, spin/parity $(59/2^-)$ has been assigned to the level at 11271.1 keV. The multipolarity for the 1022.3 keV transition could not be determined due to the presence of an overlapping γ ray in the lower part of this band.

A sequence of three γ rays of energies 988.2, 1050.4, and (1117.0) keV has been observed in coincidence with the lower part of the favored structure of band 1 feeding to $35/2$ state. We could not determine the multipolarity of any of these transitions, hence, a spin-parity assignment is missing for these states.

Band 2 was previously observed up to $I^\pi = 35/2^-$ [14]. In our work, we confirm the band and extend it up to the $47/2^-$ level by the three transitions with energies of 976.0, 1081.9, and 1158.7 keV. Spin and parity of the known levels of this band have been adopted from previous work [14]. The DCO ratios of the new transitions could not be measured due to their low intensity. We assume $E2$ multipolarity because they form a smooth continuation of the band.

The sequence of levels assigned as band 3, as shown in Fig. 2, has been established in this work. This band is decaying to the negative-parity band 1 through γ rays with energies of 1132.8 and 1288.5 keV (see Fig. 4). The DCO ratio of the 1288.5 keV transition is consistent with stretched dipole (see Table I). It is most likely stretched $E1$ transitions which favors positive parity for the levels of this band. It cannot be ruled out that it is $M1$ transition, but for such a high-energy transition one would expect sizable $E2$ admixtures, which is not reflected in the DCO ratio. The positive parity assignment to this band is also consistent with the fact that we observe a decay transition of 483.4 keV from the $27/2$ state to the $23/2^+$ level of band 5. Negative parity of band 3 would make this an $M2$ transition, which is unlikely.

The decoupled band 4 has also been established in this work. The excitation energy of the band has been fixed by the γ-ray transitions observed in coincidence with low-lying transitions of bands 1 and 3. DCO ratios measured for the in-band transitions of band 4 show their $E2$ character (see Table I). The spin assignment to the band is based on DCO ratios measured for some of the decay-out transitions that connect this band to levels of known spin and parity. In some cases unambiguous assignments are possible due to the presence of parallel transitions decaying to different levels. Positive parity is assigned to this band, as discussed further in the following paragraphs.

The level at 2706.1 keV decays through the 976.7, 1021.6, and 711.6 keV transitions to the levels with $I^\pi = 21/2^-$, $23/2^-$, and $19/2^+$, respectively. This level is populated from the $27/2^+$ state of band 3 through a γ ray of energy 598.5 keV. We have assigned spin-parity $23/2^+$ to this level because it is fed from the $27/2^+$ state and it decays to the $19/2^+$ state. The DCO ratio of the 1021.6 keV γ ray is consistent with quadrupole multipolarity. However, by assigning $23/2^+$ to this level, the 1021.6 keV γ ray becomes an unstretched $E1$ transition. Here one should note, that DCO

TABLE I. Energies, intensities, DCO ratios, and multipolarity and spin assignments of γ-ray transitions of ^{123}Cs.

E_γ[a]	Intensity[b]	DCO ratio	Assignment $J_1^\pi \rightarrow J_f^\pi$	Band	E_i	Multipolarity
224.2	32(5)	0.53(9)[c]	$25/2^+ \rightarrow 23/2^+$	$\rightarrow 5$	3045.4	$M1$
259.2	24(4)	0.62(6)	$27/2^{(+)} \rightarrow 25/2^+$	$3\rightarrow$	3304.6	$M1$
268.8	218(17)	0.75(9)	$11/2^+ \rightarrow 9/2^+$	$5 \rightarrow 5$	596.9	$M1$
280.3	8(2)		$39/2^- \rightarrow 37/2^-$	$1 \rightarrow 1$	5214.0	$M1$
284.2	22(3)	0.52(7)	$27/2^+ \rightarrow 25/2^+$	$4\rightarrow$	3329.6	$M1$
288.2	9(2)		$29/2^{(+)} \rightarrow 27/2^+$	$3 \rightarrow 4$	3617.8	$M1$
303.5	150(13)	0.62(7)[c]	$13/2^+ \rightarrow 11/2^+$	$5 \rightarrow 5$	900.4	$M1$
313.2	43(5)	0.60(6)	$29/2^{(+)} \rightarrow 27(2)^{(+)}$	$3 \rightarrow 3$	3617.8	$M1$
320.4	1000	0.93(5)	$15/2^- \rightarrow 11/2^-$	$1 \rightarrow 1$	476.7	$E2$
331.6	26(4)		$27/2^{(+)} \rightarrow 25(2)^{(+)}$	$3 \rightarrow 3$	3304.6	$M1$
334.2	3(1)		$43/2^- \rightarrow 41/2^-$	$1 \rightarrow 1$	6239.9	$M1$
336.7	133(10)	0.69(12)[c]	$15/2^+ \rightarrow 13/2^+$	$5 \rightarrow 5$	1237.1	$M1$
356.5	4(1)	0.57(7)[c]	$27/2^+ \rightarrow 25/2^{(+)}$	$4\rightarrow$	3329.6	$M1$
367.8	85(8)		$17/2^+ \rightarrow 15/2^+$	$5 \rightarrow 5$	1604.9	$M1$
371.3	2(1)		$47/2^- \rightarrow 45/2^-$	$1 \rightarrow 1$	7352.8	$M1$
377.1	46(4)	0.66(5)	$31/2^{(+)} \rightarrow 29/2^{(+)}$	$3 \rightarrow 3$	3994.9	$M1$
389.7	40(4)		$19/2^+ \rightarrow 17/2^+$	$5 \rightarrow 5$	1994.6	$M1$
398.6	34(3)		$19/2^+ \rightarrow 17/2^+$	$6 \rightarrow 5$	2003.5	$M1$
400.0	2(1)		$51/2^- \rightarrow 49/2^-$	$1 \rightarrow 1$	8559.6	$M1$
406.9	12(2)		$21/2^+ \rightarrow 19/2^+$	$5 \rightarrow 6$	2410.4	$M1$
410.8	27(3)		$23/2^+ \rightarrow 21/2^+$	$5 \rightarrow 5$	2821.2	$M1$
413.0	21(3)	0.64(7)	$33/2^{(+)} \rightarrow 31/2^{(+)}$	$3 \rightarrow 3$	4407.9	$M1$
415.8	12(2)		$21/2^+ \rightarrow 19/2^+$	$5 \rightarrow 5$	2410.4	$M1$
425.6	16(3)	0.62(8)	$35/2^{(+)} \rightarrow 33/2^{(+)}$	$3 \rightarrow 3$	4833.5	$M1$
426.5	2(1)		$55/2^- \rightarrow 53/2^-$	$1 \rightarrow 1$	9862.6	$M1$
428.0	160(15)		$11/2^+ \rightarrow 7/2^+$	$6 \rightarrow 6$	659.6	$E2$
432.7	10(2)		$23/2^+ \rightarrow 21/2^+$	$6 \rightarrow 5$	2843.1	$M1$
433.5	33(5)	0.76(6)	$19/2^- \rightarrow 17/2^-$	$2 \rightarrow 1$	1592.9	$M1$
458.5	6(2)		$39/2^{(+)} \rightarrow 37/2^{(+)}$	$3 \rightarrow 3$	5792.4	$M1$
466.5	4(1)		$23/2^- \rightarrow 21/2^-$	$2 \rightarrow 1$	2195.9	$M1$
483.4	14(3)		$27/2^{(+)} \rightarrow 23/2^+$	$3 \rightarrow 5$	3304.6	$E2$
486.7	18(4)	0.90(11)	$23/2^+ \rightarrow 19/2^+$	$\rightarrow$	2706.1	$E2$
498.0	5(1)	0.98(15)[c]	$59/2^- \rightarrow 57/2^-$	$\rightarrow 1$	11271.1	$M1$
500.4	12(3)		$37/2^{(+)} \rightarrow 35/2^{(+)}$	$3 \rightarrow 3$	5333.9	$M1$
508.4	7(2)		$27/2^+ \rightarrow 23/2^+$	$4 \rightarrow 5$	3329.6	$E2$
522.3	786(31)	0.95(10)	$19/2^- \rightarrow 15/2^-$	$1 \rightarrow 1$	999.0	$E2$
570.0	30(5)		$21/2^- \rightarrow 17/2^-$	$1 \rightarrow 1$	1729.4	$E2$
572.3	39(6)		$13/2^+ \rightarrow 9/2^+$	$5 \rightarrow 5$	900.4	$E2$
598.5	30(6)	1.16(13)	$27/2^{(+)} \rightarrow 23/2^+$	$3\rightarrow$	3304.6	$E2$
600.4	110(3)		$15/2^+ \rightarrow 11/2^+$	$6 \rightarrow 6$	1260.0	$E2$
603.0	17(3)		$23/2^- \rightarrow 19/2^-$	$2 \rightarrow 2$	2195.9	$E2$
623.5	29(4)	0.99(9)	$27/2^+ \rightarrow 23/2^+$	$4\rightarrow$	3329.6	$E2$
640.2	68(11)		$15/2^+ \rightarrow 11/2^+$	$5 \rightarrow 5$	1237.1	$E2$
644.7	48(5)	0.99(10)	$29/2^{(+)} \rightarrow 25/2^{(+)}$	$3 \rightarrow 3$	3617.8	$E2$
663.9	5(1)	0.77(10)[c]	$61/2^{(-)} \rightarrow 59/2^-$	$\rightarrow 1$	11916.9	$M1$
675.5	28(4)	0.56(6)[c]	$37/2^- \rightarrow 35/2^-$	$1 \rightarrow 1$	4933.7	$M1$
682.7	45(6)		$17/2^- \rightarrow 15/2^-$	$1 \rightarrow 1$	1159.4	$M1$
685.5	628(25)	0.98(10)	$23/2^- \rightarrow 19/2^-$	$1 \rightarrow 1$	1684.5	$E2$

TABLE I. (*Continued.*)

E_γ[a]	Intensity[b]	DCO ratio	Assignment $J_1^\pi \rightarrow J_f^\pi$	Band	E_i	Multipolarity
690.3	34(4)		$31/2^{(+)} \rightarrow 27/2^{(+)}$	$3 \rightarrow 3$	3994.9	$E2$
691.7	19(3)		$41/2^- \rightarrow 39/2^-$	$1 \rightarrow 1$	5905.7	$M1$
695.6	5(1)	1.59(25)[c]	$67/2^+ \rightarrow 63/2^+$	$4 \rightarrow 4$	13164.6	$E2$
701.9	37(5)	0.58(6)	$33/2^- \rightarrow 31/2^-$	$1 \rightarrow 1$	4055.2	$M1$
704.5	56(7)		$17/2^+ \rightarrow 13/2^+$	$5 \rightarrow 5$	1604.9	$E2$
705.0	4(1)	1.41(34)[c]	$(71/2^+) \rightarrow 67/2^+$	$4 \rightarrow 4$	13869.6	$E2$
706.9	33(4)	1.28(22)	$25/2^- \rightarrow 21/2^-$	$1 \rightarrow 1$	2436.3	$E2$
711.6	8(2)		$23/2^+ \rightarrow 19/2^+$	$\rightarrow 5$	2706.1	$E2$
715.6	66(10)	0.96(6)	$31/2^+ \rightarrow 27/2^+$	$4 \rightarrow 4$	4045.2	$E2$
721.0	10(2)		$27/2^- \rightarrow 23/2^-$	$2 \rightarrow 2$	2916.9	$E2$
730.4	99(8)	0.47(7)	$21/2^- \rightarrow 19/2^-$	$1 \rightarrow 1$	1729.4	$M1$
734.6	42(8)		$19/2^+ \rightarrow 15/2^+$	$5 \rightarrow 6$	1994.6	$E2$
740.6	11(3)		$31/2^+ \rightarrow 27/2^{(+)}$	$4 \rightarrow 3$	4045.2	$E2$
741.6	13(3)		$45/2^- \rightarrow 43/2^-$	$1 \rightarrow 1$	6981.5	$M1$
742.0	57(7)	0.48(9)	$29/2^- \rightarrow 27/2^-$	$1 \rightarrow 1$	3227.0	$M1$
743.5	37(7)		$19/2^+ \rightarrow 15/2^+$	$6 \rightarrow 6$	2003.5	$E2$
751.8	64(7)	0.35(6)	$25/2^- \rightarrow 23/2^-$	$1 \rightarrow 1$	2436.3	$M1$
757.5	41(5)		$19/2^+ \rightarrow 15/2^+$	$5 \rightarrow 5$	1994.6	$E2$
766.5	19(4)		$19/2^+ \rightarrow 15/2^+$	$6 \rightarrow 5$	2003.5	$E2$
790.1	26(4)	1.00(10)	$33/2^{(+)} \rightarrow 29/2^{(+)}$	$3 \rightarrow 3$	4407.9	$E2$
790.7	40(6)	1.35(15)	$29/2^- \rightarrow 25/2^-$	$1 \rightarrow 1$	3227.0	$E2$
800.5	389(18)	1.03(8)	$27/2^- \rightarrow 23/2^-$	$1 \rightarrow 1$	2485.0	$E2$
805.5	20(3)		$21/2^+ \rightarrow 17/2^+$	$5 \rightarrow 5$	2410.4	$E2$
806.7	6(2)		$49/2^- \rightarrow 47/2^-$	$1 \rightarrow 1$	8159.5	$M1$
811.5	8(2)		$31/2^- \rightarrow 27/2^-$	$2 \rightarrow 2$	3728.4	$E2$
817.7	–[d]		$23/2^+ \rightarrow 19/2^+$	$5 \rightarrow 6$	2821.2	$E2$
817.8	74(9)	1.12(7)	$35/2^+ \rightarrow 31/2^+$	$4 \rightarrow 4$	4863.0	$E2$
826.6	30(4)		$23/2^+ \rightarrow 19/2^+$	$5 \rightarrow 5$	2821.2	$E2$
828.2	25(4)	1.15(14)	$33/2^- \rightarrow 29/2^-$	$1 \rightarrow 1$	4055.2	$E2$
838.6	25(4)	1.44(21)	$35/2^{(+)} \rightarrow 31/2^{(+)}$	$3 \rightarrow 3$	4833.5	$E2$
839.6	9(2)		$23/2^+ \rightarrow 19/2^+$	$6 \rightarrow 6$	2843.1	$E2$
848.6	16(3)		$23/2^+ \rightarrow 19/2^+$	$5 \rightarrow 5$	2843.1	$E2$
868.3	270(14)	1.10(8)	$31/2^- \rightarrow 27/2^-$	$1 \rightarrow 1$	3353.3	$E2$
876.7	6(2)		$53/2^- \rightarrow 51/2^-$	$1 \rightarrow 1$	9436.1	$M1$
878.5	25(4)	1.13(19)	$37/2^- \rightarrow 33/2^-$	$1 \rightarrow 1$	4933.7	$E2$
888.4	57(8)	1.11(9)	$39/2^+ \rightarrow 35/2^+$	$4 \rightarrow 4$	5751.4	$E2$
892.0	6(2)		$35/2^- \rightarrow 31/2^-$	$2 \rightarrow 2$	4620.4	$E2$
904.9	197(10)	1.09(8)	$35/2^- \rightarrow 31/2^-$	$1 \rightarrow 1$	4258.2	$E2$
917.8	13(3)		$39/2^+ \rightarrow 35/2^{(+)}$	$4 \rightarrow 3$	5751.3	$E2$
918.9	41(6)	1.10(10)	$43/2^+ \rightarrow 39/2^+$	$4 \rightarrow 4$	6670.3	$E2$
926.0	14(3)		$37/2^{(+)} \rightarrow 33/2^{(+)}$	$3 \rightarrow 3$	5333.9	$E2$
955.8	145(9)	0.95(8)	$39/2^- \rightarrow 35/2^-$	$1 \rightarrow 1$	5214.0	$E2$
958.9	18(4)		$39/2^{(+)} \rightarrow 35/2^{(+)}$	$3 \rightarrow 3$	5792.4	$E2$
971.8	20(4)	1.37(31)	$41/2^- \rightarrow 37/2^-$	$1 \rightarrow 1$	5905.7	$E2$
976.0	5(1)		$39/2^- \rightarrow 35/2^-$	$2 \rightarrow 2$	5596.4	$E2$
976.3	38(5)	0.94(8)	$47/2^+ \rightarrow 43/2^+$	$4 \rightarrow 4$	7646.6	$E2$
976.7	-[d]		$23/2^+ \rightarrow 21/2^-$	$\rightarrow 1$	2706.1	$E1$
988.2	8(2)		$- \rightarrow 35/2^-$	$\rightarrow 1$	5246.4	$E2$

TABLE I. (*Continued.*)

E_γ[a]	Intensity[b]	DCO ratio	Assignment $J_1^\pi \rightarrow J_f^\pi$	Band	E_i	Multipolarity
1021.6	16(4)	1.02(15)	$23/2^+ \rightarrow 23/2^-$	$\rightarrow 1$	2706.1	$E1$
1022.3	-[d]		$63/2^- \rightarrow (59/2^-)$	$1 \rightarrow 1$	12293.5	$E2$
1025.9	104(8)	1.20(10)	$43/2^- \rightarrow 39/2^-$	$1 \rightarrow 1$	6239.9	$E2$
1040.5	5(1)		$63/2^- \rightarrow 59/2^-$	$1 \rightarrow 1$	12293.5	$E2$
1050.4	5(1)		$- \rightarrow -$	$\rightarrow 1$	6296.8	$E2$
1052.9	27(4)	1.05(9)	$51/2^+ \rightarrow 47/2^+$	$4 \rightarrow 4$	8699.5	$E2$
1059.8	7(2)	1.42(17)[c]	$63/2^- \rightarrow 59/2^-$	$1 \rightarrow 1$	12293.5	$E2$
1060.0	14(3)		$19/2^+ \rightarrow 17/2^-$	$\rightarrow 1$	2219.4	$E1$
1075.8	16(4)	0.95(19)	$45/2^- \rightarrow 41/2^-$	$1 \rightarrow 1$	6981.5	$E2$
1081.9	3(1)		$43/2^- \rightarrow 39/2^-$	$2 \rightarrow 2$	6678.2	$E2$
1102.7	4(1)		$67/2^- \rightarrow 63/2^-$	$1 \rightarrow 1$	13534.0	$E2$
1112.9	68(6)	1.03(12)	$47/2^- \rightarrow 43/2^-$	$1 \rightarrow 1$	7352.8	$E2$
1116.2	25(5)		$19/2^- \rightarrow 15/2^-$	$2 \rightarrow 1$	1592.9	$E2$
1117.0	<2		$- \rightarrow -$	$\rightarrow 1$	7413.8	$E2$
1132.8	31(5)		$29/2^{(+)} \rightarrow 27/2^-$	$3 \rightarrow 1$	3617.8	$E1$
1132.8	14(3)	1.42(21)[c]	$59/2^+ \rightarrow 55/2^+$	$4 \rightarrow 4$	11020.6	$E2$
1158.7	2(1)		$47/2^- \rightarrow 43/2^-$	$2 \rightarrow 2$	7836.9	$E2$
1178.0	19(4)	1.18(15)	$49/2^- \rightarrow 45/2^-$	$1 \rightarrow 1$	8159.5	$E2$
1178.3	7(2)		$63/2^- \rightarrow 59/2^-$	$1 \rightarrow 1$	12431.3	$E2$
1188.3	18(3)	1.56(22)[c]	$55/2^+ \rightarrow 51/2^+$	$4 \rightarrow 4$	9887.8	$E2$
1196.9	11(3)		$23/2^- \rightarrow 19/2^-$	$2 \rightarrow 1$	2195.9	$E2$
1206.8	58(5)	1.13(11)	$51/2^- \rightarrow 47/2^-$	$1 \rightarrow 1$	8559.6	$E2$
1220.4	12(3)		$19/2^+ \rightarrow 19/2^-$	$\rightarrow 1$	2219.4	$E1$
1232.4	7(2)		$27/2^- \rightarrow 23/2^-$	$2 \rightarrow 1$	2916.9	$E2$
1240.5	8(2)	1.61(23)[c]	$67/2^- \rightarrow 63/2^-$	$1 \rightarrow 1$	13534.0	$E2$
1243.4	4(1)		$31/2^- \rightarrow 27/2^-$	$2 \rightarrow 1$	3728.4	$E2$
1276.6	14(3)	1.22(30)	$53/2^- \rightarrow 49/2^-$	$1 \rightarrow 1$	9436.1	$E2$
1288.5	70(9)	0.63(7)	$25/2^{(+)} \rightarrow 23/2^-$	$3 \rightarrow 1$	2973.0	$E1$
1303.1	41(4)	1.10(15)	$55/2^- \rightarrow 51/2^-$	$1 \rightarrow 1$	9862.6	$E2$
1325.4	9(2)	1.38(26)	$59/2^+ \rightarrow 55/2^+$	$4 \rightarrow 4$	11213.4	$E2$
1337.0	8(2)		$57/2^- \rightarrow 53/2^-$	$1 \rightarrow 1$	10773.1	$E2$
1360.9	49(6)	0.66(8)	$25/2^{(+)} \rightarrow 23/2^-$	$\rightarrow 1$	3045.4	$E1$
1371.0	22(3)	1.19(7)	$59/2^- \rightarrow 55/2^-$	$1 \rightarrow 1$	11233.7	$E2$
1390.3	17(2)	0.97(9)	$59/2^- \rightarrow 55/2^-$	$1 \rightarrow 1$	11253.0	$E2$
1395.9	6(2)		$63/2^+ \rightarrow 59/2^+$	$4 \rightarrow 4$	12609.3	$E2$
1421.7	5(1)	1.63(24)[c]	$71/2^- \rightarrow 67/2^-$	$1 \rightarrow 1$	14955.6	$E2$
1448.4	11(3)	1.68(28)[c]	$63/2^+ \rightarrow 59/2^+$	$4 \rightarrow 4$	12469.0	$E2$

[a]Uncertainties in the energies of the γ ray is between 0.2 and 0.6 keV depending on their intensity.
[b]Intensities are normalized to the 320.4 keV transition with $I_\gamma = 1000$.
[c]The ratio obtained from angular distribution matrices.
[d]Measurement of intensity and DCO ratio is not possible due to presence of γ ray of overlapping energy.

ratios cannot distinguish between transitions of stretched quadrupole and unstretched dipole character. If the 1021.6 keV γ ray would be an unstretched $M1$ transition the 2706.1 keV level would have $I^\pi = 23/2^-$. However, this would then make the 711.6 and 598.5 keV γ rays $M2$ transitions, which is very unlikely.

The level at 3045.4 keV is showing decays to the $23/2^-$ state of band 1 and the $23/2^+$ state of band 5 through the 1360.9 and 224.2 keV γ rays. This level is also fed from the $27/2^+$ state of band 3 through a γ ray of 259.2 keV. The DCO ratios measured for the 259.2, 224.2, and 1360.9 keV transitions show their dipole character. Thus, spin and parity of $25/2^+$ has been assigned to the 3045.4 keV level.

Four γ rays of energies 284.2, 356.5, 508.4, and 623.5 keV have been found to decay from the level at 3329.6 keV. The DCO ratios measured for the 623.5 and 284.2 keV γ rays, which decay respectively to the $23/2^+$ and $25/2^+$ states, are consistent with quadrupole and dipole char-

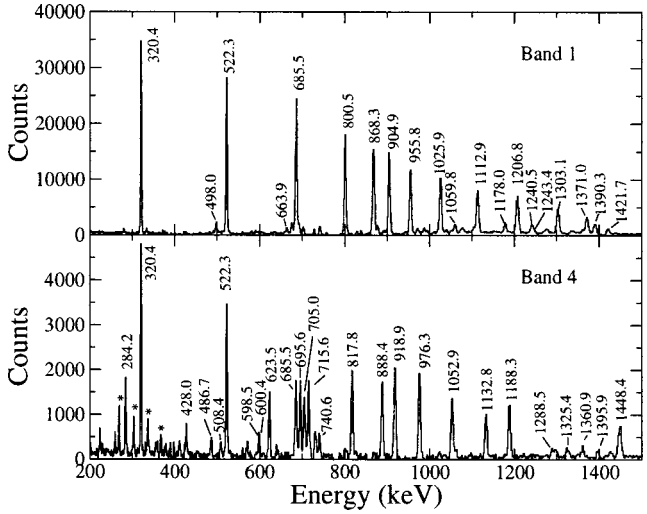

FIG. 3. Summed triple-gated γ-ray coincidence spectra of band 1 (upper panel) and of band 4 (lower panel). For band 1, gates were set on all γ rays of the favored $\alpha=-1/2$ signature band, whereas for band 4 gates were set on all the γ-ray transitions. The peaks marked with asterisks (lower panel) belong to band 5 observed in coincidence with band 4.

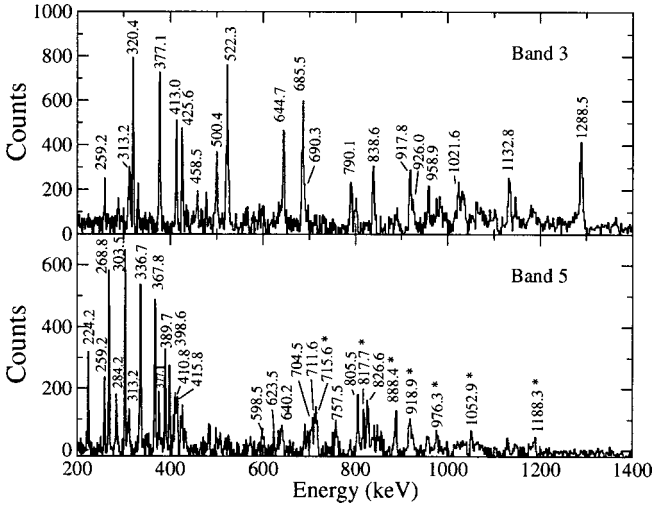

FIG. 4. Summed triple-gated γ-ray coincidence spectra of band 3 (upper panel) and of band 5 (lower panel). The upper spectrum was produced by setting two gates on the transitions of 644.7, 377.1, 413.0, 425.6, 500.4, and 458.5 keV of band 3 and one gate on any of the 320.4, 522.3, and 685.5 keV transitions of band 1. The lower spectrum was obtained by setting triple gates on any of the transitions with energies of 268.8, 303.5, 336.7, 367.8, 389.7, 410.8, and 415.8 keV of band 5. The γ rays marked by asterisks (lower panel) belong to band 4 observed in coincidence with band 5.

acter, respectively. Thus, we have assigned spin-parity $27/2^+$ to the level at 3329.6 keV. The observation of other decays further support the assignment of positive parity to band 4.

In Fig. 3, an example of the spectra obtained by setting triple gates on all the γ-ray transitions of band 4 is shown. The γ rays belonging to band 5 as well as some of the linking transitions are clearly visible in coincidence with those of band 4. Similar to band 1, band 4 also forks into two structures at spin $55/2^+$, as shown in Fig. 2 by the sequences 4a and 4b. The intensity ratio of the 1132.8 and 1325.4 keV transitions is around 1.6, which shows that above spin 55/2, structure 4b of this band is yrast and more strongly populated. The transitions in sequence 4b are irregular in energy. They have been ordered according to their intensities (see Table I). The DCO ratios measured for the transitions in sequence 4b are consistent with their $E2$ multipolarity. However, due to the large uncertainty in the DCO ratio for the 705.0 keV γ ray a tentative spin $(71/2^+)$ has been assigned to the highest level of structure 4b. Sequence 4a is extended by $E2$ transitions up to a $63/2^+$ level.

The coupled band 5 (see Fig. 2), was already reported in the previous in-beam studies [13–15]. In the first two of these investigations an excitation energy of 296 keV was reported for the $9/2^+$ level, which is the band-head of this band. However, this was not confirmed by the recent work of Gizon *et al.* [21]. An excitation energy of 231.6+X, where X is few tenths of a keV, was suggested for this level. Furthermore, these authors have measured a lifetime of 114 ns for the $9/2^+$ state using a recoil-catcher technique. In the present work, we have observed the transitions with energies of 224.2, 483.4, and 508.4 keV decaying from bands 3 and 4, as well as the 711.6 keV γ ray from the level at 2706.1 keV in coincidence with γ rays of band 5 (see Fig. 4). On the basis of these linking transitions we propose the level at 328.1 keV as the state $9/2^+$. Gizon *et al.* [21] also have placed a level at 328.1 keV which decays through the 96.5 and 233.5 keV γ rays to the $7/2^+$ and $5/2^+$ levels at 231.6 and 94.6 keV, respectively. However, they could not measure their multipolarity and, hence, spin-parity values of $5/2^+$ or $7/2^+$ were tentatively assigned to this level. In this experiment, we do not observe the 233.5 and 94.6 keV transitions depopulating 328.1 keV level. For a state with a lifetime of 114 ns we do not expect to observe these transitions because a thin target was used in this experiment, in which the nuclei were recoiling into vacuum after the reaction and the evaporation residues decay out of the focal plane of the collimated detectors.

The 428.0, 600.4, and 743.5 keV transitions which constitute band 6 were also known from previous studies [13,14]. However, its excitation energy was uncertain [14]. Gizon *et al.* [21] have firmly established the level at 231.6 keV with spin and parity $7/2^+$. We have placed band 6 on top of this level. The placement of the band is further supported by the fact that we observe a number of interband transitions between bands 5 and 6 (see Fig. 2).

IV. DISCUSSION

In this section we will discuss the configurations of the bands. Arguments for the configuration assignments are the observed band-crossing frequencies and alignment gains in comparison to those observed in the neighboring nuclei as well as comparison to theoretical calculations. For the high-spin states, calculations have been performed using the configuration-dependent cranked Nilsson-Strutinsky (CNS) formalism [10,22]. In this formalism, the different configurations are identified by the number of particles in the

N-shells of the rotating basis. The different orbitals are identified and particles in high-j intruder shells and in the other j-shells can be distinguished [23,24]. The configurations are then labeled by the number of particles in the different j-shells or groups of j-shells. In the case of the ^{123}Cs, it is natural to label the configurations relative to a ^{114}Sn core, i.e., by the number of proton holes in the $g_{9/2}$ orbitals, the number of protons in the $h_{11/2}$ subshell, and the number of neutrons in the $h_{11/2}$ subshell. The number of protons and neutrons in the low-j $N=4$ orbitals $(g_{7/2},d_{5/2},d_{3/2},s_{1/2})$ is then determined from the fixed number of protons and neutrons, $Z=55$ and $N=68$. We note, however, that in this formalism the separation of nucleons into core and valence particles is artificial. In the numerical calculations no core is introduced, and all orbitals (up to $N=8$) are treated on the same footing. For the sake of simplicity the shorthand notation $[(p_0)p_1,n]$ is used for labeling the configurations, where p_0 is the number of proton holes in the $g_{9/2}$ orbitals (omitted when $p_0=0$), p_1 is the number of $h_{11/2}$ protons and n is the number of $h_{11/2}$ neutrons. The energy of each configuration at each spin is minimized in the deformation space $(\varepsilon_2,\varepsilon_4,\gamma)$, which allows the development of collectivity within specific configurations to be traced as a function of spin. Pair correlations are neglected in the calculations. Thus, they can be considered as realistic only at high spins. In the calculations, we have used the so called "$A=130$ parameters," previously applied to the superdeformed and highly deformed bands in the Ce/Nd nuclei [25] and to the high-spin bands in La nuclei [26,27]. In the present application, in which only valence space configurations are considered, these parameters are essentially identical to the parameters which have been used for the terminating bands in $A\approx 110$ nuclei [10].

A. Band 1

The negative-parity band 1 is the most intensely populated band in this nucleus. It consists of two signature-partner branches of $\Delta I=2$ transitions starting from spin $11/2^-$ and $17/2^-$ corresponding to signatures $\alpha=-1/2$ and $\alpha=1/2$, respectively. A large signature splitting ($\simeq$350 keV at $\hbar\omega\simeq 350$ keV) is observed in the lower part of the band which indicates involvement of a rotation-aligned low-Ω particle in the configuration. The configuration of this band has been discussed in previous work [13–15]. It was suggested that it involves the proton $[550]1/2^-$ orbital of $h_{11/2}$ origin, which is in agreement with the observed signature splitting. In Fig. 5, the dynamic moments of inertia for band 1 are plotted as a function of rotational frequency. It experiences a band crossings at frequencies of 0.44 and 0.41 MeV for the favored and unfavored signatures, respectively. This crossing has been explained by the alignment of a pair of $h_{11/2}$ neutrons [14,15]. The first $h_{11/2}$ proton crossing is blocked by the odd $[550]1/2^-$ proton. In the neighboring even-even core nucleus ^{122}Xe, the first $h_{11/2}$ neutron crossing in the ground-state band has been observed at $\hbar\omega\simeq 0.38$ MeV [3]. The observed delay of this crossing in ^{123}Cs can be attributed to the deformation driving effect of the $[550]1/2^-$ proton.

The alignment i_x for band 1 is plotted as a function of rotational frequency in the Fig. 6. The Harris-expansion [28] parameters, $J_0=17.0\ \hbar^2\ \mathrm{MeV}^{-1}$ and $J_1=25.8\ \hbar^4\ \mathrm{MeV}^{-3}$, have been adopted from previous work [14]. An alignment gain of $\simeq 5\hbar$ is observed in the crossing. A similar gain in alignment of 6.1 $\hbar$ has been reported for the $h_{11/2}$ neutron crossing in ^{122}Xe [3].

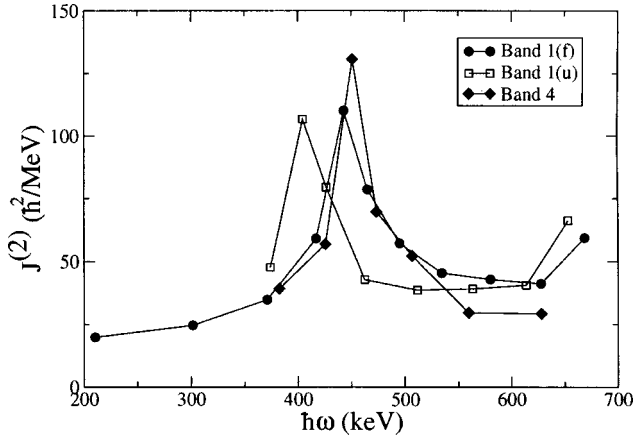

FIG. 5. Dynamic moments of inertia $J^{(2)}$ as a function of rotational frequency for bands 1 and 4. Favored (unfavored) signature partners of band 1 are labeled f(u).

An interesting structure appears in band 1 above spin $55/2$. Two or possibly three levels with spin $59/2$, and two levels with spin $63/2$ are observed. These higher-spin states can be grouped into two sequences, labeled 1a and 1b, respectively, in the level scheme of Fig. 2. They show decays into each other by γ rays which are irregular in energy and are probably a mixture of collective as well as single-particle excitations. Irregular structures have been observed already at lower spin values in the even-even core nucleus ^{122}Xe [3]. They have been interpreted as favored noncollective states, based on partially aligned configurations, e.g., $\pi[(g_{7/2}d_{5/2})^2_6(h_{11/2})^2_{10}]_{16}\otimes\nu[(h_{11/2})^4]_8$ for $I^\pi=24^+$, and then reaching the fully aligned valence-space configurations around $I=30$, e.g., $\pi[(g_{7/2}d_{5/2})^2_6(h_{11/2})^2_{10}]_{16}\otimes\nu[(h_{11/2})^4]_{16}(I^\pi=32^+)$ and $\pi[(g_{7/2}d_{5/2})^2_6(h_{11/2})^2_{10}]_{16}\otimes\nu[(h_{11/2})^3_{13.5}(d_{3/2})^1_{1.5}]_{15}(I^\pi=31^-)$ [3].

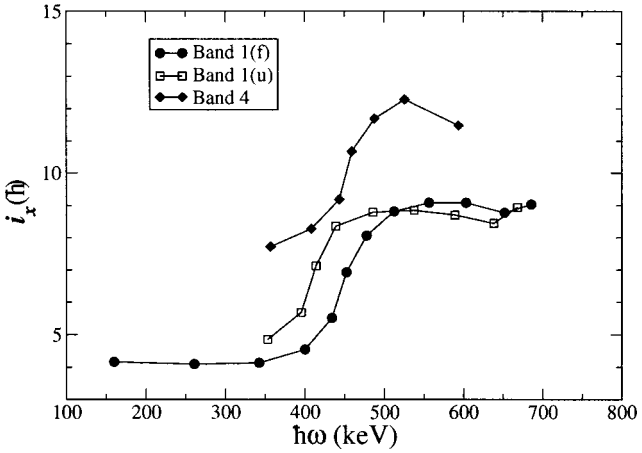

FIG. 6. Rotation alignment as a function of rotational frequency for bands 1 and 4. Favored (unfavored) signature partners of band 1 are labeled f(u).

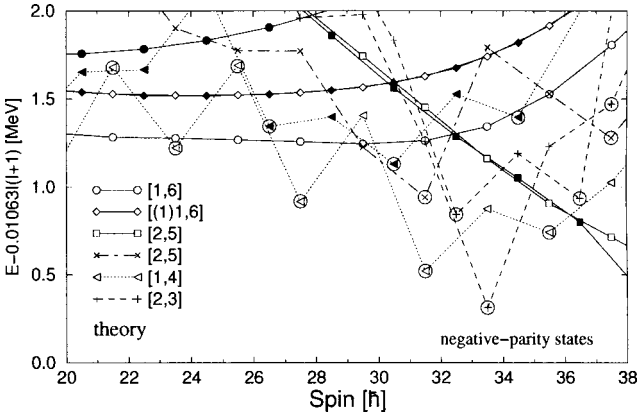

FIG. 7. Calculated excitation excitation energies relative to a rigid-rotor reference as a function of spin for the lowest energy configurations in the framework of CNS model. Solid and open symbols represent signature $\alpha=1/2$ and $\alpha=-1/2$ states, respectively.

In order to interpret the high-spin states in ^{123}Cs, calculations within the framework of the CNS model have been performed. In Fig. 7 calculated excitation energies relative to a rigid-rotor reference for the lowest-energy negative-parity configurations are plotted as a function of spin in the high-spin region. The $\alpha=-1/2$ and $\alpha=1/2$ signature states are labeled by open and full symbols, respectively. The configurations are labeled only for one of the two signatures in the legend, however, both the open and full version of the same symbol correspond to the same configuration. The most striking feature of the calculation is that two different types of configurations compete in the spin region considered. There are regular band structures and other states with irregular energy spacings. The states with the regular pattern are connected by solid lines in the plot. They have collective character with shape parameters ε_2 between 0.2 and 0.3, and γ close to zero. The states belonging to the irregular patterns are connected by dotted lines in Fig. 7. They are noncollective or close to noncollective with shape parameters ε_2 less than 0.2 and γ approaching 60°. The noncollective states with $\gamma=60°$ are encircled in the plots.

The regularity of a configuration is related to the number of holes in the $N=64$ neutron core. No holes in the core corresponds to a minimal number of active valence particles and thus to configurations that are irregular and less collective. In these configurations, either all four valence neutrons are in the $h_{11/2}$ subshell or one of them is in the $d_{3/2}$ subshell instead. With holes in the neutron core, as in the cases when the $h_{11/2}$ subshell contains six neutrons, the configuration is regular and more collective. According to the calculations the collective configurations generally compete successfully with the noncollective ones below spin ≈ 30, while above this spin the noncollective configurations lie more and more at lower energy. This feature seems to be reflected well by the experimental observations. Analogous features are found e.g., in the $Z=68$ nucleus ^{158}Er [11,12] where collective bands with six $h_{11/2}$ protons are yrast up to $I\approx 40$, but they are then crossed by less collective configurations with a closed $Z=64$ core (four $h_{11/2}$ protons), which then build the favored $I=46$ fully aligned state (see Fig. 1).

Among the calculated negative-parity bands the $\alpha=-1/2$ signature branch of the [1,6] configuration, i.e., the $\pi h^1_{11/2} \otimes \nu^6_{11/2}$ structure, is yrast up to spin 28. The positive signature of this configuration is predicted to lie about 500 keV higher in energy. The experimental yrast band 1 has a large signature splitting with a favored $\alpha=-1/2$ signature branch lower in energy. It was already mentioned that the lower-spin part of band 1 has been previously assigned as the $h_{11/2}$ proton configuration. We assign the $\pi h^1_{11/2} \otimes \nu h^6_{11/2}$ configuration to the high-spin part of the band. However, the predicted signature splitting is much larger than the observed one. In the calculation the favored signature branch is predicted to have a prolate shape with $\gamma \simeq 0$, while the predicted shape of the unfavored branch is triaxial with $\gamma \simeq -30°$. There is a secondary minimum for the favored branch in the calculations with γ close to −30°. This minimum is considerably closer in energy to the unfavored branch in agreement with the experimental observation. Therefore, band 1 may correspond to the [1,6] configuration, having triaxial shape with $\gamma \simeq -30°$. The predicted yrare configuration in this spin region is the [(1)1,6], i.e., the $\pi[g^{-1}_{9/2} h^1_{11/2}] \otimes \nu h^6_{11/2}$ configuration, which has no signature splitting. However, no such band has been observed in the experiment.

Around spin 30 the experimental band pattern changes. There are several states with the same spin, and the slope of the energy as a function of spin changes. This is in agreement with the calculations, which predict that in this region the [1,4] and [2,3], i.e., the $\pi h^1_{11/2} \otimes \nu h^4_{11/2}$ and $\pi h^2_{11/2} \otimes \nu h^3_{11/2}$ noncollective configurations, respectively, become yrast. The $\alpha=-1/2$ signature states are predicted to be energetically strongly favored, and to form a down-sloping pattern. The $\alpha=-1/2$ signature branch of the [2,3] configuration is predicted to have a very favored state at spin $67/2$, but at other spin values this configuration lies well above the yrast line. Therefore, it cannot correspond to the experimental structures 1a and 1b which have favored states in the spin range $63/2$ and $71/2$. The [1,4] configuration, however, can account for the observed bands.

In Fig. 8 we compare the observed bands with the predicted [1,6] and [1,4] configurations. The [1,4] configuration contains four $h_{11/2}$ neutrons while the distribution of neutrons between orbitals of $g_{7/2}d_{5/2}$ and $d_{3/2}s_{1/2}$ character might vary. Depending on this distribution, different minima are formed in the potential energy surfaces for the [1,4] configuration as illustrated in Fig. 9. The closed-core configuration (with no $d_{3/2}s_{1/2}$ neutrons) is built in the minimum labeled A. The corresponding energy curve drawn in Fig. 8 terminates in a very favored $63/2^-$ state.

In Fig. 8 we have also plotted the band with two holes in the $g_{7/2}d_{5/2}$ orbitals of the [1,4] configuration which consequently has two neutrons in $d_{3/2}s_{1/2}$. This band is relatively easy to follow because in the potential energy surface of Fig. 9, it corresponds to the minimum labeled C. Furthermore, also the two highest-spin states of the [1,4] band with one $g_{7/2}d_{5/2}$ hole shows up as minima in the potential energy surfaces (labeled B in Fig. 9). The corresponding energy values are drawn in Fig. 8. The lower spin values of the corresponding band are too high in energy to show up as local minima in the potential energy surfaces but they are expected

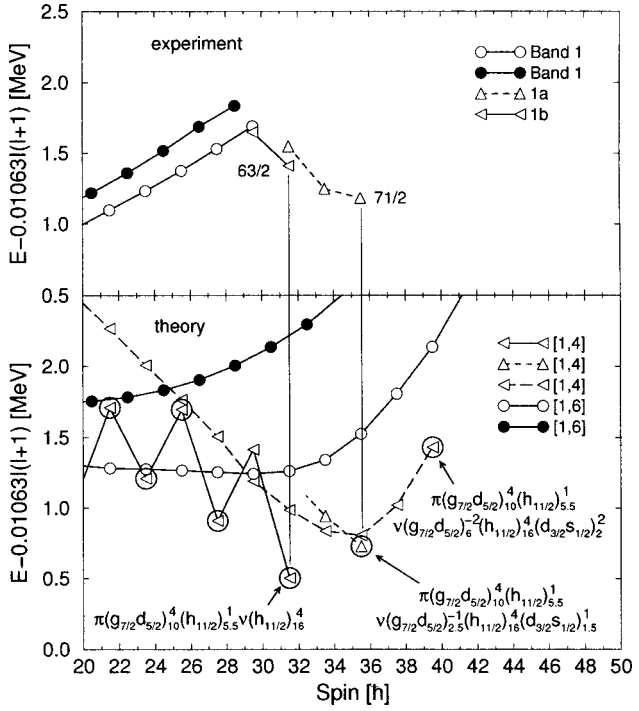

FIG. 8. Experimental excitation energies relative to a rigid-rotor reference as a function of spin for band 1 (upper panel) and the calculated values for the [1,4] and [1,6] configurations (lower panel) in the framework of CNS model. Noncollective aligned states are encircled and the precise filling of orbitals with dominant components in specific subshells is spelled out for the fully aligned states.

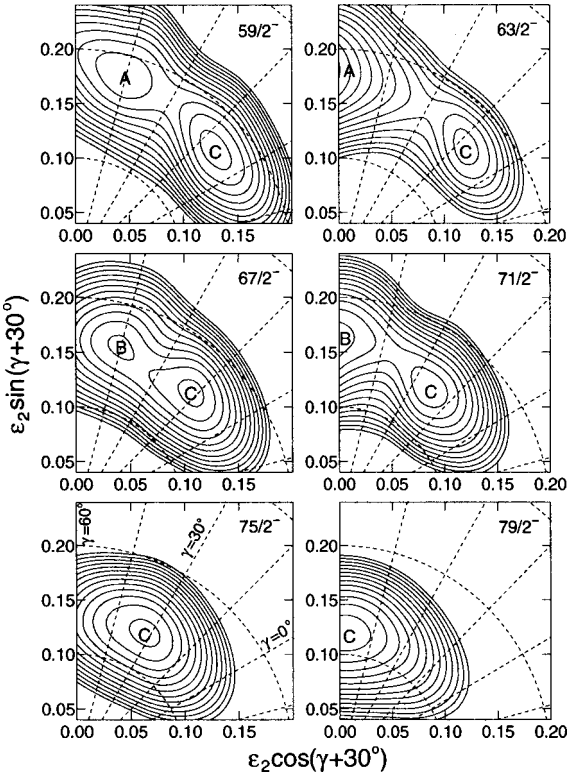

FIG. 9. Calculated potential energy surfaces in the (ε_2, γ)-plane for the [1,4], i.e., $\pi(h_{11/2})^1\nu(h_{11/2})^4$ configuration of ^{123}Cs. The γ values are defined in the lower left panel where $\gamma=0°$ corresponds to collective rotation at prolate shape and $\gamma=60°$ corresponds to noncollective rotation at oblate shape. Different local minima are formed depending on the number of neutrons excited from the $g_{7/2}d_{5/2}$ orbitals of the $N=64$ core to the $d_{3/2}s_{1/2}$ orbitals. With a closed core, minimum A is formed that terminates at $I=63/2$, and with one particle excited, minimum B is formed, which is only seen for $I=67/2$ and for the terminating spin $I=71/2$. On the other hand, the evolution of minimum C, corresponding to two excited particles, can be followed for all spin values shown, when it smoothly loses collectivity and ends up in the terminating $I=79/2$ state.

to follow a more or less smooth trend. According to Fig. 8, the structure 1a can be assigned either to the [1,4] configuration with one neutron in the $d_{3/2}s_{1/2}$ subshell, which is predicted to terminate at spin $71/2$, or to the [1,4] configuration with two neutrons in the $d_{3/2}s_{1/2}$ subshell, which is predicted to be more collective, and its termination spin is $79/2$. In the first case the highest-spin state of structure 1a is a terminating state. However, the observed smooth behavior and the relative positions of the states in the sequence favors the second assignment. Further experimental investigations of the higher-spin states connected to structure 1a would be needed to distinguish between the two possibilities.

In the calculations, also the $55/2^-$ state of the [1,4] configuration is noncollective and is energetically favored. However, considering the relative position of the [1,6] and [1,4] states in general, it appears questionable if this state should really be expected to be yrast. Furthermore, it is not fully aligned and therefore more uncertain. Thus, it is certainly not strange that no state corresponding to this calculated $55/2^-$ has been observed. We can also note that a third $59/2^-$ state has been drawn in Fig. 2 which is, however, dependent on the unknown ordering of the 498.0 and 1022.3 keV transitions; if this ordering was changed, a $61/2^-$ state would show up in the level scheme instead. Assuming the ordering in Fig. 2, the $59/2^-$ state could be assigned as built mainly on [1,4] configuration (see Fig. 8).

In order to illustrate the precise configurations of the highest-spin states, the Nilsson single-particle energy levels (e_i) are plotted as a function of spin-projection quantum number (m_i) in Fig. 10. The straight lines drawn through the plots represent the slope of the tilted Fermi surface (see, Refs. [29,30]). The calculated shape parameters $\varepsilon_2=0.19$, $\gamma=60°$ are typical values at termination of the valence space configurations. In the "optimal" configurations, corresponding to the minimum energy configurations at given spins, the occupied Nilsson single-particle states lie below the tilted straight lines in the e_i-m_i plane. For other fillings in which the occupied orbitals cannot be placed below a tilted Fermi surface, the energy will in general be higher relative to the yrast line. The spin values in specific configurations can be obtained by summing the m_i values of the occupied states. The occupied and empty states of the specific ^{123}Cs configurations are denoted by filled and empty circles, respectively. Thus, in the right-hand panels of Fig. 10, proton and neutron orbitals involved in the $63/2$ state of the [1,4] configuration are shown by filled circles. In the standard notation they correspond to the $\pi[h^1_{11/2}(d_{5/2}g_{7/2})^4]\otimes\nu(h_{11/2})^4$ configuration. If a neutron from $g_{7/2}$ $(m_i=-5/2)$ is excited to $d_{3/2}(m_i$

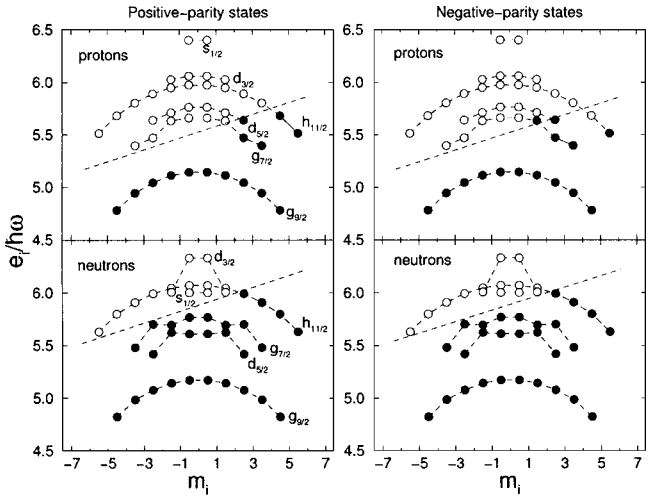

FIG. 10. The single-particle energies (e_i) as a function of spin-projection quantum number (m_i) calculated at shape parameters $\varepsilon_2=0.19$, $\gamma=60°$. The straight lines drawn through the plots represent approximate tilted Fermi surfaces for the terminating configurations [1,4] (negative-parity states) and [2,4] (positive-parity states) of ^{123}Cs in the case with no holes in the core. The filling of the orbitals in these specific states is indicated by the filled circles below the tilted straight lines.

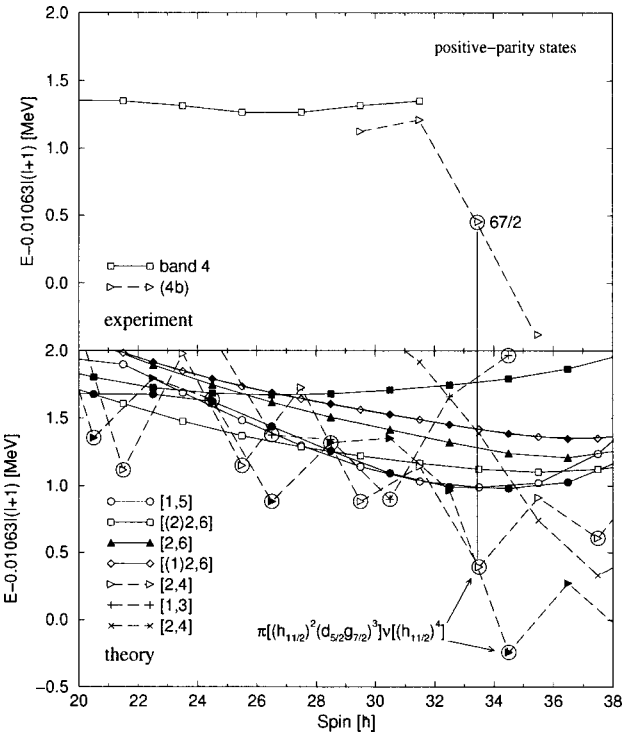

FIG. 11. Experimental excitation energies relative to a rigid-rotor reference as a function of spin for band 4 (upper panel) and the calculated values for different configurations (lower panel) in the framework of the CNS model. The solid and open symbols represent the favored and unfavored signature states of the specified configurations, respectively.

$=3/2$) (see right panel of Fig. 10), we obtain the terminating state at spin $71/2$ of the [1,4] configuration with one neutron hole in the core. Similarly, if one more neutron is excited from $g_{7/2}$ ($m_i=-7/2$) to $d_{3/2}$ ($m_i=1/2$), we obtain the terminating state with spin $79/2$ of the [1,4] configuration with two neutron holes in the core. As discussed above, these configurations are alternative interpretations of the highest observed negative-parity states (see Fig. 8).

As a final comment on the high-spin negative-parity states, we note that the specific arrangement of the states into structures 1a and 1b is somewhat arbitrary, which also means that the interpretation presented here could be modified. On the other hand, the experimental feature that the energies start to decrease at $I\approx 30$ when drawn versus the standard reference, and its interpretation in terms of a transition to configurations terminating in the spin range $I=30-40$, is clearly independent of such details. Furthermore, considering that band 1 is interpreted in terms of a configuration with an even number of neutrons in the $h_{11/2}$ orbital, this is certainly what is expected also for the less collective high-spin states, leaving the [1,4] configuration as the only reasonable interpretation of the higher spin states. These neutron configurations for $N=68$ are in agreement with the general features for the terminating bands observed in Dy/Er nuclei ($Z=66-68$) in analogous configurations with a few neutrons or protons outside a core with 64 particles (see e.g., Refs. [11,12]).

B. Band 4

The excitation energy of the band-head and the initial alignment observed for the positive-parity band 4 are consistent with a three-quasiparticle configuration. The large alignment (see Fig. 6) can be obtained only if low-Ω, high-j particles are involved. The dynamic moments of inertia $J^{(2)}$ for this band, plotted in Fig. 5, show that it experiences a band crossing at a rotational frequency of 0.45 MeV, similar to that of the favored sequence of band 1, which is due to the alignment of a pair of $h_{11/2}$ neutrons. The alignment gain of $\simeq 5\hbar$ due to this crossing is very similar to that observed in band 1. The observation of the $h_{11/2}$ neutron crossing makes it very unlikely that an odd number of $h_{11/2}$ neutrons is involved in the configuration below this crossing.

CNS calculations have been made for different configurations for positive-parity states. In Fig. 11 calculated excitation energies relative to a rigid-rotor reference are displayed along with the experimental energies for band 4. According to the calculations, the lowest-energy configurations involve proton excitations from the $g_{9/2}$ orbital across the $Z=50$ shell gap. As shown in Fig. 11, the $\alpha=-1/2$ signature of the [(2)2,6] configuration, i.e., the $\pi[(g_{9/2}^{-2})h_{11/2}^2]\otimes\nu h_{11/2}^6$ structure, appears lowest in energy in the spin range 20 to 28. The positive-parity [2,6], i.e., the $\pi h_{11/2}^2\otimes\nu h_{11/2}^6$ configuration, which does not involve particle-hole excitations across the $Z=50$ gap, appears in the calculation at higher energy. This may be due to the deformation driving effect of the $g_{9/2}$ proton holes which lowers the energy of the core-excited configuration. There are two other collective configurations predicted near the yrast line, the [1,5] ($\pi h_{11/2}^1\otimes\nu h_{11/2}^5$) and the [(1)2,6] ($\pi[g_{9/2}^1 h_{11/2}^2]\otimes\nu h_{11/2}^6$) configurations. Both of these are predicted to have very small signature splitting. Noncollective states corresponding to the [2,4] ($\pi h_{11/2}^2$

$\otimes \nu h_{11/2}^4$) configuration appear favored in the calculations throughout the studied spin region. However, they are irregular in energy and no yrast $E2$-transition cascade can be formed between these states below spin $59/2$.

Experimentally, we observe only $\alpha=-1/2$ signature states of band 4 and do not observe the other signature partner. This suggests that the signature splitting is large and the unfavored branch lies high above the yrast line and is too weakly populated to be detected in this experiment. Thus, we can rule out the configurations [1,5] ($\pi h_{11/2}^1 \otimes \nu h_{11/2}^5$) and [(1)2,6] $\pi[(g_{9/2}^{-1}h_{11/2}^2] \otimes \nu h_{11/2}^6$) which show small signature splitting. The observation of the $h_{11/2}$ neutron crossing in band 4, as mentioned above, also goes against assigning the [1,5] ($\pi h_{11/2}^1 \otimes \nu h_{11/2}^5$) configuration to this band since this crossing would be blocked for this configuration. Both of the other two configurations, i.e., the [2,6] ($\pi h_{11/2}^2 \otimes \nu h_{11/2}^6$) and [(2)2,6] $\{\pi[(g_{9/2}^{-2})h_{11/2}^2] \otimes \nu h_{11/2}^6\}$ structures, show large signature splitting. of about 500 keV but with the opposite signature favored. Thus, it is only for the [(2)2,6] configuration that the observed signature is calculated lowest in energy. The calculation predicts larger deformation for the [(2)2,6] $\{\pi[(g_{9/2}^{-2})h_{11/2}^2] \otimes \nu h_{11/2}^6\}$ configuration ($\varepsilon_2 \simeq 0.3$) compared to that for the [2,6] ($\pi h_{11/2}^2 \otimes \nu h_{11/2}^6$) configuration ($\varepsilon_2 \simeq 0.2$). Based on the similarities observed between the experimental features and the calculated [(2)2,6] configuration, we suggest that band 4 above the crossing may have the [(2)2,6] $\{\pi[(g_{9/2}^{-2})h_{11/2}^2] \otimes \nu h_{11/2}^6\}$ configuration. This assignment is further supported by the fact that this band shows a decay to the $\pi g_{9/2}^{-1}$ band 5 as well as to $\pi h_{11/2}$ band 1. However, we cannot rule out other possibilities, keeping in mind the uncertainties of the relative excitation energies in the calculation.

Neutron crossing frequencies are sensitive to the deformation. It has been found from systematic studies that with increasing deformation the neutron crossing frequency is increasing [1]. The calculated deformation associated with the positive-parity [2,6] configuration is similar to that associated with the negative parity band 1, whereas it is larger for the [(2)2,6] configuration compared to the other two. Experimentally, we observe the crossing in both bands 1 and 4 at the same frequency, which suggests similar deformations for these bands. This favors the configuration [2,6] for band 4. We note here that although the predicted favored signature branch of this configuration is the opposite to the observed one in band 4, this fact is not a strong argument against the [2,6] configuration assignment. Indeed, in the [2,6] and [(2)2,6] configurations the calculated signature splitting depend on the chosen Nilsson parameters, thus, they can even be reversed in another parametrization. It would be helpful to have a lifetime measurement for the bands from which the quadrupole moments could be deduced.

At spin $55/2$, band 4 forks into two structures, labeled in Fig. 2 as 4a and 4b, respectively. The smooth variation in γ-ray energy of the sequence labeled 4a can be viewed as continuation of the band. However, this configuration is no longer yrast at spin $59/2^+$ and most of the intensity flow is coming through the other structure labeled 4b, which is sharply down-sloping when drawn as in Fig. 11. These general features are reproduced by the calculations in which the [2,4] configuration comes down in energy around these spin values. Indeed, the excitation energy of the lowest $59/2^+$, $63/2^+$, and $67/2^+$ states relative to that of band 4 is in good agreement with the states of the [2,4] configuration in the calculation (see Fig. 11). The tilted Fermi surface diagram for the [2,4] configuration is shown in the left-hand panel of Fig. 10. From this figure we can derive the single-partical configuration of the $69/2$ state as the terminating state of the [2,4] $\{\pi[h_{11/2}^2(g_{7/2}d_{5/2})^3] \otimes \nu h_{11/2}^4\}$ configuration. The $67/2$ state of this configuration can be obtained by exciting a proton from the $d_{5/2}$ ($m_i=5/2$) state to the $9_{7/2}$ ($m_i=3/2$) state.

Assuming that the tentative spin of the highest state of the side band is correct, i.e., $71/2^+$, it might be interpreted as belonging to a [2,4] configuration with one or two neutrons excited from $g_{7/2}$ to $d_{3/2}$. Indeed, the neutron configuration is identical for the [2,4] positive parity and for the [1,4] negative parity structures, so that they should have analogous features displaced by $3\hbar$ which is the difference in maximal spin for the $\pi[(h_{11/2})^1(d_{5/2}g_{7/2})^4]_{15.5}$ and $\pi[(h_{11/2})^2(d_{5/2}g_{7/2})^3]_{18.5}$ proton configurations (see Fig. 10). For the [1,4] structures, we found bands with one and two neutrons excited from $g_{7/2}$ to $d_{3/2}$ at similar energies as the closed core band (see Fig. 8). Thus, we expect analogous bands in the [2,4] configuration, i.e., an $1p$-$1h$ band terminating at $I^\pi=75/2^+$ (drawn as the [2,4] band in Fig. 11 for spin values $71/2$ and $75/2$) and a $2p$-$2h$ band terminating at $I^\pi=83/2^+$. Both of these bands are then expected to have relatively low-lying lower-spin states, in which one of the $I^\pi=71/2^+$ states could be a candidate for the tentatively observed $71/2^+$ state. However, with this interpretation, it is difficult to understand the strongly favored character of this $71/2$ state. Alternatively, if the highest energy positive parity state would have spin $69/2$ instead, it would be naturally explained as the maximum spin state of the closed core [2,4] configuration, i.e., the most favored calculated state drawn in Fig. 11.

C. Bands 3 and 5

The two coupled bands, band 3 and band 5, show no or very small signature splitting. This indicates that high-K orbitals may be involved in the configurations. The only high-K orbital available at prolate deformation around $\varepsilon_2 \simeq 0.2-0.3$ is proton $g_{9/2}$, which is upsloping from below the shell gap at $Z=50$. The configuration of band 5 has been assigned in the previous work as $\pi g_{9/2}^{-1}$ [14,15]. Alignments for this band are plotted in Fig. 12. No sudden alignment is observed, however, there is an upsloping tendency. It is difficult to guess about the nature of the aligning particles without the complete knowledge of the full gain in alignment.

The $B(M1)/B(E2)$ ratios derived from the $\Delta I=1/\Delta I=2$ γ-ray branching ratios for band 5 are displayed in Fig. 13. They are compared to the ratios calculated using an extended formulation [31] of the geometrical model of Dönau [32] and Frauendorf [33]. In the calculation the $E2/M1$ mixing ratios for the dipole transitions have been assumed to be zero. A 15%–20% mixing for the $\Delta I=1$ transitions, however, as observed in the previous work [14], will not change the values much since it appears in the formula as δ^2. The rotational gyromagnetic factor g_R has been taken as $Z/A=0.447$ and

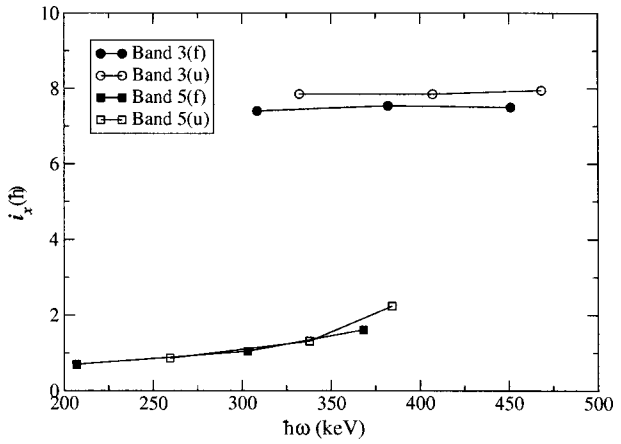

FIG. 12. Alignment (i_x) as a function of rotational frequency for bands 3 and 5. Favored (unfavored) signature branches are labeled f(u).

the relevant empirical g_K factors for the different single particles have been taken from Refs. [34,35]. The quadrupole moment, $Q_0=4.6\ b$, which corresponds to a deformation parameter of $\beta_2=0.25$ ($\beta_4=0.02$) has been taken from Refs. [15]. Axial symmetry was assumed for both bands 3 and 5.

As is evident from Fig. 13, the calculated $B(M1)/B(E2)$ ratios for the configuration $\pi g_{9/2}^{-1}$ agree reasonably well with the experimental values for band 5. At the highest frequencies there is an increase that indicates an onset of a configuration change.

Band 3 starts at a rather high spin of $27/2$. The alignment plot for this band (see Fig. 12) shows a large initial alignment which remains constant with increasing frequency. The initial alignment is similar to that observed for band 1 after the neutron crossing and is also close to the initial alignment of band 4. This indicates that band 3 has a three-quasiparticle configuration involving aligned high-j orbitals like $h_{11/2}$. The most probable configurations may be $\pi g_{9/2}^{-1}\otimes\pi h_{11/2}^{2}$, $\pi g_{9/2}^{-1}\otimes\nu h_{11/2}^{2}$ or $\pi[g_{9/2}^{-1}h_{11/2}^{1}]\otimes\nu h_{11/2}^{1}$. The $B(M1)/B(E2)$ ratios are rather sensitive to the configuration in which neutron or proton $h_{11/2}$ orbitals are involved. The ratios have been calculated for the above mentioned configurations and are compared the experimental results in Fig. 13. It is clear that we can rule out the configuration involving two aligned quasiprotons in the $h_{11/2}$ orbital. The configuration involving two neutrons in the $h_{11/2}$ orbital is most favored. However, the possibility of the $\pi[g_{9/2}^{-1}h_{11/2}^{1}]\otimes\nu h_{11/2}^{1}$ configuration, involving one quasiparticle both from proton and neutron in the $h_{11/2}$ orbital cannot be ruled out.

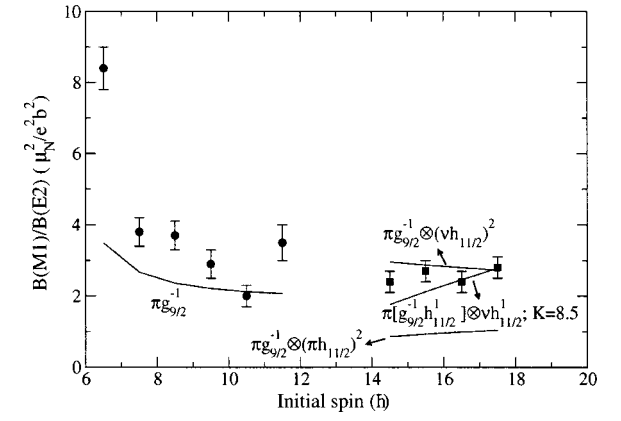

FIG. 13. $B(M1)/B(E2)$ ratios derived from the γ-ray branching ratios for band 3 (squares) and band 5 (circles). Calculated values for different configurations using the geometrical model of Dönau and Frauendorf are shown by the curves.

Band 6 has already been observed in the previous work [14] and the configuration has been discussed. It was assigned a configuration involving $g_{7/2}$ proton orbitals. At higher spin, both bands 5 and 6 interact strongly and show transitions between each other.

V. SUMMARY

The results obtained from a high-spin study of ^{123}Cs using the Gammasphere spectrometer array have been presented. The four previously known bands have been extended to higher spins and two additional bands have been established. Irregular structures due to noncollective excitation have been observed at very high spin in two of the bands. States have been identified in the $I=30-35$ spin range that are energetically favored by about 1.0–1.5 MeV relative to the smooth trends defined by the collective bands below $I\approx 30$. These specific features are explained in configuration-dependent cranked Nilsson-Strutinsky calculations in which configurations based on a closed $^{114}_{50}\mathrm{Sn}_{64}$ core or with one or two particle-hole excitations relative to this core become energetically favored around $I=30$. Specific observed states are thus identified with calculated maximalspin aligned states built on the valence-space configurations, $\pi[h_{11/2}^{1}(g_{7/2}d_{5/2})^4]$ or $\pi[h_{11/2}^{2}(g_{7/2}d_{5/2})^3]$ combined with the $\nu[h_{11/2}]^4$ configuration. In addition, another band structure is assigned as being part of a terminating band built on a closed shell proton configuration but with one or two neutrons excited across the $N=64$ shell gap. On the other hand, no experimental counterpart to the calculated highest-spin closed-core state at $I=69/2^+$ has been identified and no theoretical counterpart could be identified to the highest-spin state observed experimentally. The latter spin assignment is, however, tentative and further experimental and theoretical studies appear necessary to resolve these issues.

ACKNOWLEDGMENTS

We wish to thank the staff of the Berkeley Cyclotron for providing the beams and we greatly appreciate the support obtained from the staff involved in running the Gammasphere spectrometer. The work was supported by BMBF (Germany) under the Contract No. 06 BN 907 and by DFG under Contract No. HU 325/10, Danish Natural Science Research Council, the Swedish Science Research Council, the Hungarian Scientific Research Fund, OTKA (Contract No. T046901), and the Bolyai János Foundation, and the U. S. Department of Energy under Contract No. DE-AC03-76SF00098.

[1] R. Wyss, *et al.*, Nucl. Phys. **A505**, 337 (1989).
[2] A. Granderath, P. F. Mantica, R. Bengtsson, R. Wyss, P. von Brentano, A. Gelberg, and F. Seiffert, Nucl. Phys. **A597**, 427 (1996).
[3] H. Timmers, J. Simpson, M. A. Riley, T. Bengtsson, M. A. Bentley, F. Hanna, S. M. Mullins, J. F. Sharpey-Schafer, and R. Wyss, J. Phys. G **20**, 287 (1994).
[4] Y. Liang *et al.*, Phys. Rev. C **44**, R578 (1991).
[5] S. Törmänen *et al.*, Nucl. Phys. **A613**, 282 (1997).
[6] E. S. Paul. J. Simpson, S. Araddad, C. W. Beausang, M. A. Bentley, M. J. Joyce, and F. Sharpey-Secharfer, J. Phys. G **19**, 913 (1993).
[7] D. L. Balabanski *et al.*, Phys. Rev. C **56**, 1629 (1997).
[8] S. Juutinen *et al.*, Z. Phys. A **338**, 365 (1991).
[9] J. Timár, J. Simpson, E. S. Paul, S. Araddad, C. W. Beausang, M. A. Bentley, M. J. Joyce, and J. F. Sharpey-Schafer, J. Phys. G **21**, 783 (1995).
[10] A. V. Afansjev, D. B. Fossan, G. J. Lane, and I. Ragnars, Phys. Rep. **322**, 1 (1999), and references therein.
[11] I. Ragnarsson, Z. Xing, T. Bengtsson, and M. A. Riley, Phys. Scr. **34**, 651 (1986).
[12] J. Simpson *et al.*, Phys. Lett. B **327**, 187 (1994).
[13] U. Garg, T. P. Sjoreen, and D. B. Fossan, Phys. Rev. C **19**, 217 (1979).
[14] J. R. Hughes, D. B. Fossan, D. R. LaFosse, Y. Liang, P. Vaska, M. P. Waring, and J.-Y. Zhang, Phys. Rev. C **45**, 2177 (1992).
[15] F. Lidén *et al.*, Nucl. Phys. **A550**, 365 (1992).
[16] D. C. Radford, Nucl. Instrum. Methods Phys. Res. A **361**, 297 (1995).
[17] G. Beyer, A. Jasiński, O. Knotek, H.-G. Ortlepp, H.-U. Siebert, R. Arlt, E. Hermann, G. Musiol, and J. Tyroff, Nucl. Phys. **A260**, 269 (1976).
[18] P. Arlt, A. Jasinski, W. Neubert, and H.-G. Ortlepp, Acta Phys. Pol. B **6**, 433 (1975).
[19] D. D. Bogdanov, A. V. Demyanov, V. A. Karnaukhov, M. Nowick, L. A. Petrov, J. Voboil, and A. Plochock, Nucl. Phys. **A307**, 421 (1978).
[20] G. Marguier, A. Charvet, J. Genevey, C. Richard-Serre, A. Knipper, and G. Walter, J. Phys. G **7**, 101 (1981).
[21] A. Gizon *et al.*, Eur. Phys. J. A **8**, 41 (2000).
[22] T. Bengtsson and I. Ragnarsson, Nucl. Phys. **A436**, 14 (1985).
[23] I. Ragnarsson, V. P. Janzen, D. B. Fossan, N. C. Schmeing, and R. Wadsworth, Phys. Rev. Lett. **74**, 3935 (1995).
[24] A. V. Afanasjev and I. Ragnarsson, Nucl. Phys. **A591**, 387 (1995).
[25] A. V. Afanasjev and I. Ragnarsson, Nucl. Phys. **A608**, 176 (1996).
[26] C. M. Parry *et al.*, Phys. Rev. C **61**, 021303(R) (2000).
[27] R. Wadsworth *et al.*, Phys. Rev. C **62**, 034315 (2000).
[28] S. M. Harris, Phys. Rev. **138**, B509 (1965).
[29] G. Andersson *et al.*, Nucl. Phys. **A268**, 205 (1976).
[30] M. J. A. DeVoigt, J. Dudek, and Z. Szymanski, Rev. Mod. Phys. **55**, 949 (1983).
[31] V. P. Janzen *et al.*, Phys. Rev. C **45**, 613 (1992).
[32] F. Dönau, Nucl. Phys. **A471**, 469 (1987).
[33] S. Frauendorf, Phys. Lett. **100B**, 219 (1981).
[34] T. Lönnroth, S. Vajda, O. C. Kistnerand, and M. H. Rafailovich, Z. Phys. A **317**, 215 (1984).
[35] D. Ward *et al.*, Z. Phys. A **529**, 315 (1991).